$K_S^0\Sigma^0$ photoproduction at the BGO-OD experiment

Katrin Kohl[1,*] *Stefan* Alef[1], *Patrick* Bauer[1], *Reinhard* Beck[2], *Alessandro* Braghieri[13], *Philip* Cole[3], *Rachele* Di Salvo[4], *Daniel* Elsner[1], *Alessia* Fantini[4,5], *Oliver* Freyermuth[1], *Francesco* Ghio[6,7], *Anatoly* Gridnev[8], *Daniel* Hammann[1], *Jürgen* Hannappel[1], *Thomas* Jude[1], *Nikolay* Kozlenko[8], *Alexander* Lapik[9], *Paolo* Levi Sandri[10], *Valery* Lisin[9], *Giuseppe* Mandaglio[11,12], *Roberto* Messi[4,5], *Dario* Moricciani[4], *Vladimir* Nedorezov[9], *Dmitry* Novinsky[8], *Paolo* Pedroni[13], *Andrei* Polonski[9], *Björn-Eric* Reitz[1], *Mariia* Romaniuk[4], *Georg* Scheluchin[1], *Hartmut* Schmieden[1], *Victorin* Sumachev[8], *Viacheslav* Tarakanov[8], and *Christian* Tillmanns[1]

[1]Rheinische Friedrich-Willhelms-Universität Bonn, Physikalisches Institut, Nußallee 12, 53115 Bonn, Germany
[2]Helmholtz-Institut fuer Strahlen- und Kernphysik, Universitaet Bonn, Nussallee 1-16, D-53115 Bonn Germany
[3]Lamar University, Department of Physics, Beaumont, Texas, 77710, USA
[4]INFN Roma Tor Vergata, Rome, Italy
[5]Università di Roma "Tor Vergata", Via della Ricerca Scientifica 1, 00133 Rome, Italy
[6]INFN sezione di Roma La Sapienza, P.le Aldo Moro 2, 00185 Rome, Italy
[7]Istituto Superiore di Sanita, Viale Regina Elena 299, 00161 Rome, Italy
[8]Petersburg Nuclear Physics Institute, Gatchina, Leningrad District, 188300, Russia
[9]Russian Academy of Sciences Institute for Nuclear Research, prospekt 60-letiya Oktyabrya 7a, Moscow 117312, Russia
[10]INFN - Laboratori Nazionali di Frascati, Via E. Fermi 40, 00044 Frascati, Italy
[11]INFN sezione Catania, 95129 Catania, Italy
[12]Universita degli Studi di Messina, Via Consolato del Mare 41, 98121 Messina, Italy
[13] INFN sezione di Pavia, Via Agostino Bassi, 6 - 27100 Pavia, Italy

Abstract.
The BGO-OD experiment at the ELSA accelerator facility uses an energy tagged bremsstrahlung photon beam to investigate the excitation structure of the nucleon via meson photoproduction.
The setup with a BGO calorimeter surrounding the target and an open dipole spectrometer covering the forward region is ideally suited for investigating low momentum transfer processes, in particular in strangeness photoproduction.
The associated photoproduction of K_S^0 and hyperons is essential to understand the role of K^* exchange mechanisms. A cusp-like structure observed in the $\gamma p \to K_S^0\Sigma^+$ reaction at the K^* threshold is described by models including dynamically generated resonances from vector meson-baryon interactions. Such interactions are predicted to give a peak like structure in $K_S^0\Sigma^0$ photoproduction off the neutron. A very preliminary cross section is determined and compared to the prediction, the results appear to support the model.

1 Introduction

The cusp-like structure observed in the $\gamma p \to K^0\Sigma^+$ differential cross section by Ewald et al. [1] is not described in previous isobar and PWA models, for example SAID [2] and K-MAID [3]. It could be described however using an equivalent model to the one that predicted the charmonium-pentaquark candidate [4] observed by the LHCb collaboration [5] in 2015 which includes dynamically generated resonances from vector meson-baryon interactions [6]. Below K^* threshold, an intermediate $K^*\Lambda$ or $K^*\Sigma$ state feeds the cross section by conversion to the final state via pion exchange. Above threshold the K^* can be produced freely. Whereas this produces a cusp in $K^0\Sigma^+$ photoproduction due to destructive interference, constructive interference is predicted to give an enhancement in $K^0\Sigma^0$ photoproduction. Fig. 1 shows both cases for two different parameter sets. The upper plot includes the experimental data from the CBELSA/TAPS collaboration [1]. A measurement of the $\gamma n \to K^0\Sigma^0$ cross section and an observation of the predicted enhancement would strongly support this theory and help with the understanding of pentaquark states.

2 BGO-OD experiment

The BGO-OD experiment at the ELSA accelerator facility in Bonn is ideally suited to measure strangeness photoproduction, especially in the very forward region. ELSA provides an electron beam up to 3.2 GeV. Via bremsstrahlung a real photon beam is produced. By measuring the momentum of the electron, the energy of the photon can be calculated.

*e-mail: kohl@physik.uni-bonn.de

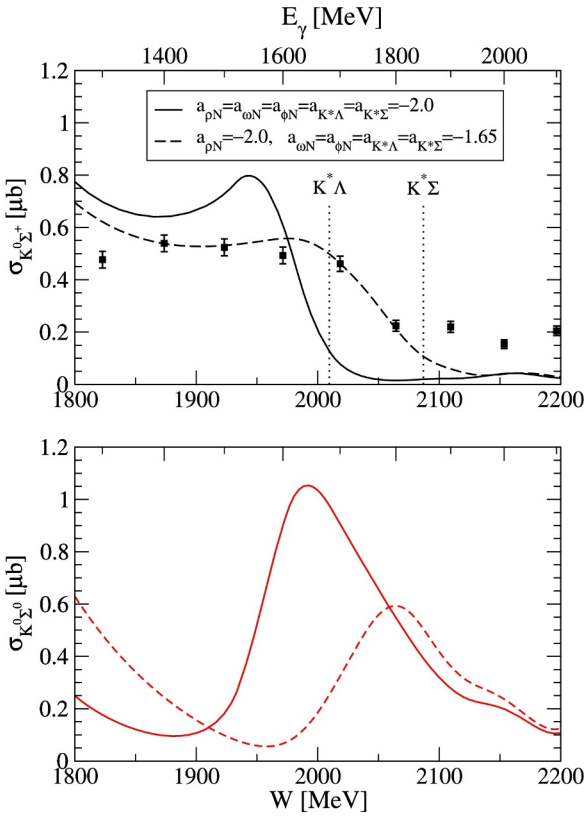

Figure 1. A prediction of the cross section of $\gamma p \rightarrow K^0\Sigma^+$ (upper plot) and $\gamma n \rightarrow K^0\Sigma^0$ (lower plot) is shown as solid line. The dotted line parameters were fitted to the data (black points [1]). Figure taken from Ref. [6].

The photon beam impinges on a fixed target, usually liquid hydrogen or deuterium. This is surrounded by a Multi-Wire-Proportional-Chamber for tracking, a scintillator barrel to provide charge information and an electromagnetic calorimeter made from BGO. This central detector is ideally suited for photon detection, but also able to detect other charged or neutral particles.

In the forward direction two tracking detectors (MOMO and SciFi) in front and eight driftchambers behind an open dipole magnet, together with time of flight measurement, allow excellent particle identification. The intermediate range is covered by SciRi, a Scintillating Ring detector, which provides directions of charged particles. An overview is given in figure 2, for detailed information on the performance of the BGO-OD experiment see Ref. [7].

3 Reconstruction

To determine a cross section of $\gamma n \rightarrow K^0\Sigma^0$ the decay channel $K^0\Sigma^0 \rightarrow \pi^0\pi^0\Lambda\gamma \rightarrow 5\gamma\Lambda$ is identified, by requesting exactly five neutral and any number of charged particle. The Λ is not reconstructed. The five photons are identified in the BGO-Ball and combined to two π^0 with one remaining photon. All combinations are allowed where no photon is used twice and the invariant masses of the π^0 are within ±25 MeV of the nominal π^0 mass. If the remaining photon is from the Σ^0 decay (for details see section 3.1), the pair of π^0 are kept and the masses are set to the nominal π^0 mass. A cut on the missing mass to $2\pi^0$ is applied at ±50 MeV around the Σ^0 mass. A plot of the invariant mass of $2\pi^0$ with these selections is shown in figure 3. A signal peak at around the K^0 mass is visible, but superimposed with a lot of background.

Using simulated data, the dominant background channels proved to be:

- $\gamma N \rightarrow 3\pi N$
- $\gamma N \rightarrow \eta N$
- $\gamma N \rightarrow \eta\pi N$
- $\gamma n \rightarrow K^0\Lambda$
- $\gamma p \rightarrow K^0\Sigma^+$

The last two are the most crucial ones, since they contribute to the signal peak. To remove part of this background the entire proton contamination is subtracted (see

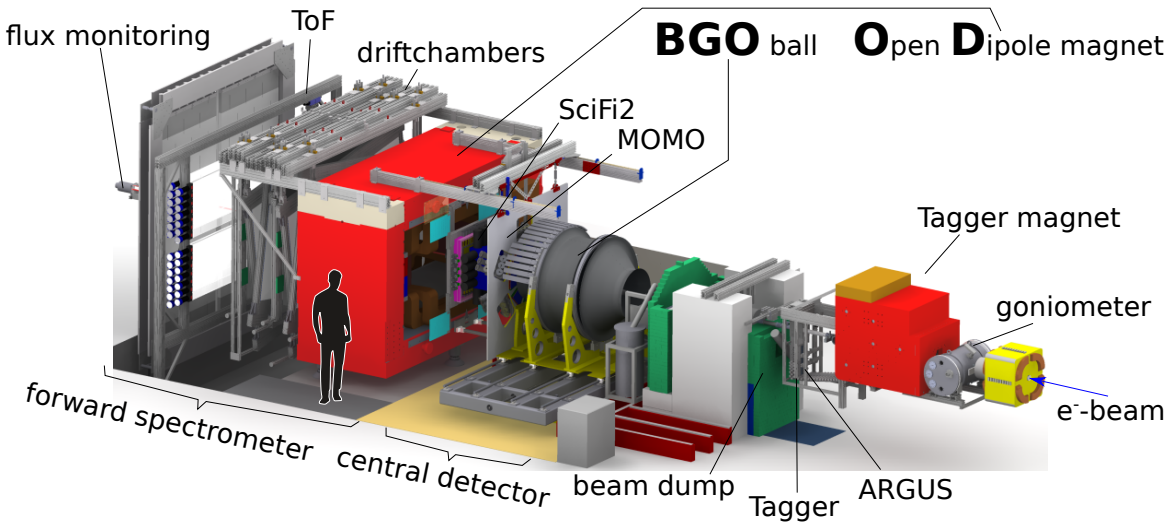

Figure 2. Overview of the BGO-OD experiment.

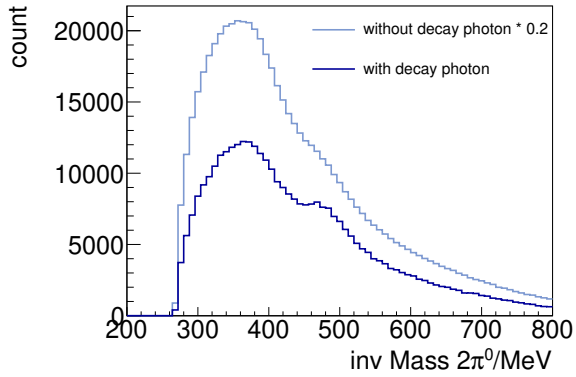

Figure 3. $2\pi^0$ invariant mass spectrum before and after selecting Σ^0 decay photon.

section 3.2). Finally the Root tool Roofit[8] is used to determine the number of signal events from the $2\pi^0$ invariant mass spectrum (section 3.3).

3.1 Tagging Σ^0 decay photon

To suppress background, the decay of the Σ^0 to a Λ and a photon was identified. In the rest frame of the Σ^0, the photon always has a constant energy of approximately the mass difference between Σ^0 and Λ of 75 MeV. Figure 4 shows the energy spectrum of a fifth photon in the BGO-calorimeter that was not used for the two π^0 reconstruction.A small peak is visible over a large background. Also shown is simulated $K^0\Sigma^0$ data, where the peak is immediately visible. To prove this technique the channel $K^+\Sigma^0$ was selected, making use of the much cleaner signal. It is evident, that in all three cases the peak in photon energy is at the same position.

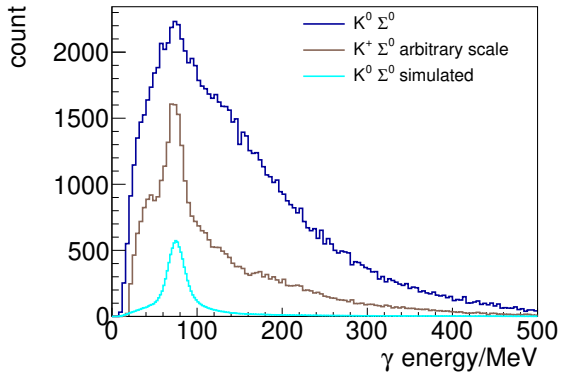

Figure 4. Energy spectrum of the Σ^0 decay photon for real and simulated data. To prove the technique is working correctly the channel $K^+\Sigma^0$ is studied.

By selecting events where this photon has an energy between 50 MeV and 105 MeV, the signal to background ratio is improved as shown in figure 3 which shows the $2\pi^0$ invariant mass spectrum. This does not only improve the signal to background ratio in general, but it also strongly suppresses the background channel $\gamma n \to K^0\Lambda$ which contributes to the signal peak, but is undesired. Only about 10% of this background channel survives, which will later be subtracted (see section 4).

3.2 Proton contamination

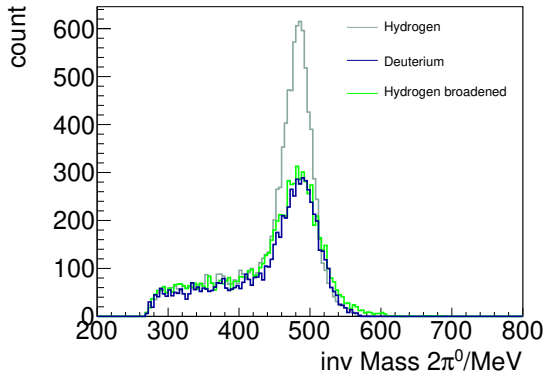

Figure 5. $2\pi^0$ invariant mass spectrum for simulated $\gamma p \to K^0\Sigma^+$ on hydrogen and deuterium target, as well as the hydrogen data set broadened according to the momentum distribution of nucleons in deuterium.

The liquid deuterium target consists of neutrons and protons. Since the investigated reaction only happens on the neutron, all reactions happening on the proton are background that have to be subtracted. This is done by doing the same analysis as before with a hydrogen target data set, which is broadened according to the momentum distribution of nucleons in deuterium. To get the correct amount of proton reactions in the deuterium data set, the hydrogen data set is scaled with the ratio of the photon flux.

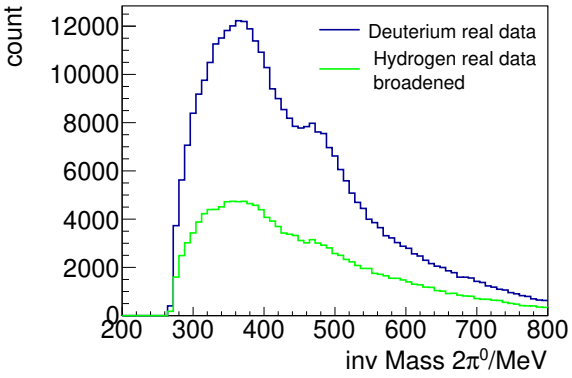

Figure 6. $2\pi^0$ invariant mass spectrum for deuterium data and broadened and scaled hydrogen data. The hydrogen data make up about half of the deuterium data.

Figure 5 shows the $2\pi^0$ invariant mass spectrum for simulated $\gamma p \to K^0\Sigma^+$ on hydrogen and deuterium targets, as well as the hydrogen data set broadened according

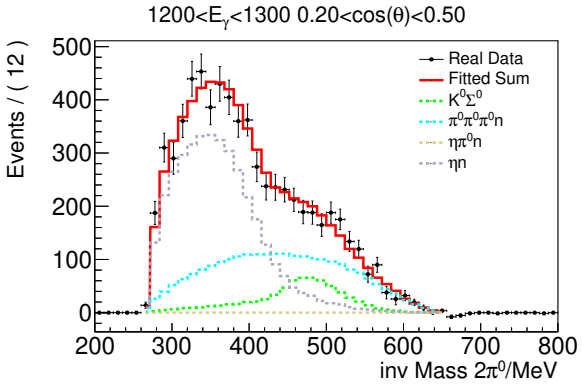

Figure 7. Example fit to $2\pi^0$ invariant mass spectrum. Simulated contributions to the fit labeled inset.

to the momentum distribution of nucleons in deuterium, after a cut on the missing mass to the $2\pi^0$ system, selecting the Σ^+. The broadening of the missing mass causes a decrease in statistic after this cut. Deuterium and broadened hydrogen data agree very well.

Figure 6 shows the $2\pi^0$ invariant mass spectrum for real data for deuterium and scaled and broadened hydrogen target data. The hydrogen target data set accounts for about half of the deuterium data set which could be expected considering the dominant background channels are uncorrelated π^0 and η production. What remains after subtraction are pure neutron channels, therefore also the background channel $\gamma n \to K^0\Sigma^+$ does not contribute to the signal peak anymore.

3.3 Fitting to data

The remaining background can be removed using the Root tool Roofit [8]. Phase space generated distributions of background channels and signal are fitted to the data. The amplitudes of the contributions are varied until the sum agrees to the data. Fig. 7 shows an example. Only points larger zero are taken into account. The spectrum is well described over the entire range and signal and background can be accurately separated. The tool allows to extract the yield of the single channels, the corresponding error bars include statistics and fit quality.

4 Differential cross section measurement

The extracted number of K^0 events is plotted as a function of beam energy in four bins in $\cos(\theta_{CM})$ in figure 8, where θ_{CM} is the center of mass polar angle. This is not the desired cross section yet, since there is still some contribution of $\gamma n \to K^0\Lambda$. To remove this contribution, the known cross section [9] is scaled with the respective reconstruction efficiency and also shown in figure 8. Within the error bars the calculated $K^0\Lambda$ contribution is in agreement with being smaller/equal than the measured yield as it is expected. After subtracting the $\gamma n \to K^0\Lambda$ contribution, a preliminary differential cross section of $\gamma n \to K^0\Sigma^0$ is shown in figure 9. Also included in this figure is the prediction by Oset and Ramos [6] in an arbitrary scale. It should be noted that this is the integrated cross section, not the plotted differential, scaled by a factor $\frac{1}{3}$ or $\frac{1}{2}$, depending on the angular region. From the integration of the solid angle a factor 2 is expected to the total cross section, which is consistent with the used scaling factors. The general shape and position of the predicted enhancement seem to agree to these preliminary results.

5 Conclusion

The results shown in figure 9 appear to support the model behind the prediction made for the cross section $\gamma n \to K^0\Sigma^0$ [6]. The general shape and position of the enhancement agree very well. More over, the enhancement appears to get stronger for more forward directions, as did the drop in the corresponding proton channel $\gamma p \to K^0\Sigma^+$ [1]. At this point it would be interesting to compare the results to predictions for the differential cross sections. Further plans are expanding the acceptance region to more forward angles, for example with the charged K^0 decay in the forward spectrometer.

This work was supported by the Deutsche Forschungsgemeinschaft project numbers 388979758 and 405882627. Our Russian collaborators thank the Russian Scientific Foundation (grant RSF number 19-42-04132) for financial support.

References

[1] R. Ewald et al., Phys. Lett. B **713**, 180 (2012)
[2] http://gwdac.phys.gwu.edu (27.8.2019)
[3] https://maid.kph.uni-mainz.de (27.8.2019)
[4] J.J. Wu, R. Molina, E. Oset, B.S. Zou, Phys. Rev. Lett. **105**, 232001 (2010)
[5] R. Aaij et al., Phys. Rev. Lett. **115**, 072001 (2015)
[6] A. Ramos and E. Oset, Phys. Lett. B **727**, 287 (2013)
[7] S. Alef et al, To be submitted to Eur. Phys. J. A (2019)
[8] W. Verkerke and D. P. Kirkby, eConf C **0303241** (2003) MOLT007 [physics/0306116].
[9] N. Compton et al Phys. Rev. C **96**, 065201 (2017)

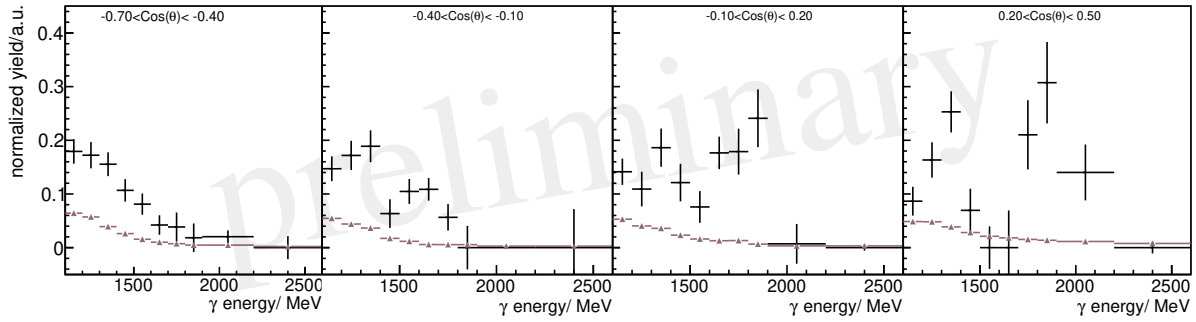

Figure 8. K^0 yield extracted from Roofit[8] (black points). Remaining $K^0\Lambda$ contribution, calculated from [9] (brown triangles). The error bars on the x-axis represent the bin width.

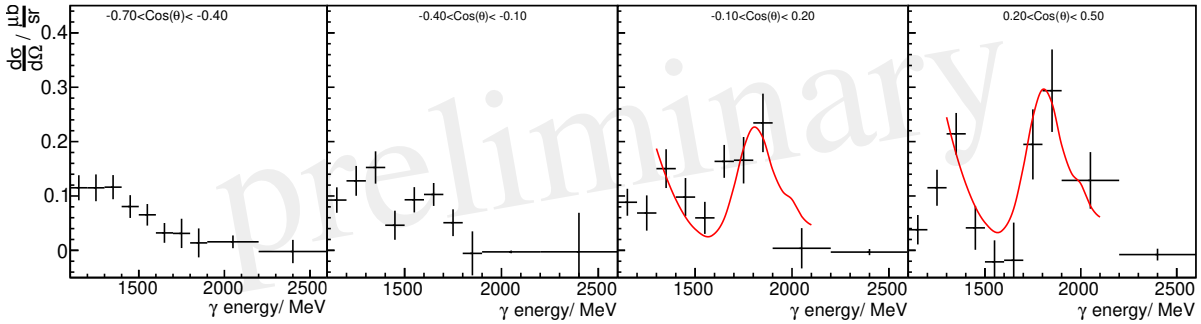

Figure 9. $\gamma n \rightarrow K^0\Sigma^0$ differential cross section (black points). Predicted enhancement by Oset and Ramos[6] in an arbitrary scale (red line). The error bars on the x-axis represent the bin width.